



On the robustness of predictions of sea level fingerprints

Citation

Mitrovica, J. X., N. Gomez, E. Morrow, C. Hay, K. Letychev, and M. E. Tamisiea. 2011. "On the Robustness of Predictions of Sea Level Fingerprints." *Geophysical Journal International* 187 (2): 729–42. <https://doi.org/10.1111/j.1365-246x.2011.05090.x>.

Published version

<https://doi.org/10.1111/j.1365-246X.2011.05090.x>

Link

<http://nrs.harvard.edu/urn-3:HUL.InstRepos:41401407>

Terms of use

This article was downloaded from Harvard University's DASH repository, and is made available under the terms and conditions applicable to Other Posted Material (LAA), as set forth at

<https://harvardwiki.atlassian.net/wiki/external/NGY5NDE4ZjgzNTc5NDQzMGIzZWZhMGFIOWI2M2EwYTg>

Accessibility

<https://accessibility.huit.harvard.edu/digital-accessibility-policy>

Share Your Story

The Harvard community has made this article openly available.

Please share how this access benefits you. [Submit a story](#)

On the robustness of predictions of sea level fingerprints

J. X. Mitrovica,¹ N. Gomez,¹ E. Morrow,¹ C. Hay,² K. Letychev² and M. E. Tamisiea³

¹Department of Earth & Planetary Sciences, Harvard University, 20 Oxford Street, Cambridge, MA 02138, USA. E-mail: jxm@eps.harvard.edu

²Department of Physics, University of Toronto, Toronto, ON M5S 1A7, Canada

³National Oceanographic Centre, Joseph Proudman Building, 6 Brownlow St., Liverpool, L3 5DA, UK

Accepted 2011 May 20. Received 2011 May 20; in original form 2010 July 5

SUMMARY

The rapid melting of the Earth's ice reservoirs will produce geographically distinct patterns of sea level change that have come to be known as sea level fingerprints. A basic, gravitationally self-consistent theory for computing these patterns appeared in the 1970s; however, recent, highly discrepant fingerprint calculations have led to suggestions that the algorithms and/or theoretical implementation adopted in many previous predictions is not robust. We present a suite of numerical predictions, including benchmark comparisons with analytic results, that counter this argument and demonstrate the accuracy of most published predictions. Moreover, we show that small differences apparent in calculations published by some groups can be accounted for by subtle differences in the underlying physics. The paper concludes with two sensitivity analyses: (1) we present the first-ever calculation of sea level fingerprints on earth models with 3-D variations in elastic structure and density, and conclude that this added complexity has a negligible effect on the predictions; (2) we compare fingerprints of polar ice sheet mass flux computed under the (very common) assumption of a uniform melt distribution to fingerprints calculated using melt geometries constrained by analysing recent trends in GRACE gravity data. Predictions in the near field of the ice sheets are sensitive to the assumed melt geometry; however, this sensitivity also extends to the far field, particularly in the case of Antarctic mass changes, because of the strong dependence of the rotational feedback signal on the melt geometry. We conclude that inferences of ice sheet mass flux based on modern sea level constraints should consider these more realistic melt geometries.

Key words: Sea level change; Earth rotation variations; Dynamics of lithosphere and mantle; Antarctica; Arctic region.

1 INTRODUCTION

To our knowledge, Woodward (1888) was the first to demonstrate that the rapid melting of an ice sheet would lead to a geographically variable sea level change. Woodward (1888) assumed a rigid, non-rotating Earth, and therefore self-gravitation of the surface load was the only contributor to the predicted departure from a geographically uniform (i.e. eustatic) sea level rise. This departure was large and counter-intuitive. Specifically, sea level was predicted to fall within ~2000 km of a melting ice sheet, and to rise with progressively higher amplitude at greater distances. The physics governing this redistribution is straightforward. An ice sheet exerts a gravitational attraction on the surrounding ocean. If the ice sheet melts, the net volume of water in the oceans increases, but the gravitational force exerted by the (now smaller) ice sheet on the ocean decreases. The latter leads to a migration of water from the near field of the ice sheet to the far field. Within 2000 km of the ice sheet, this migration dominates the sea level redistribution and the net result is a sea level fall. In the far field the migration adds to the general

increase in ocean volume, leading to a sea level rise in excess of the eustatic.

The first gravitationally self-consistent treatment of sea level change appeared in the canonical study of Farrell & Clark (1976). They treated the case of a deformable, non-rotating earth model with fixed shoreline geometry. Their theory was ultimately aimed at predicting ice age sea level changes on a viscoelastic Earth, but they explicitly considered a special, elastic case of their 'sea level equation' that would be appropriate for a rapid ice melting scenario (see their figs 3 and 4).

The Farrell & Clark (1976) equation was adopted by Clark & Lingle (1977), who were the first to consider sea level changes associated with the potential melting of polar ice due to global warming. In particular, they computed the sea level change associated with a uniform thinning of the West Antarctic Ice Sheet (WAIS). Their result, reproduced in Fig. 1(a), was normalized by the eustatic sea level change (i.e. the change computed assuming that the meltwater entered the present-day ocean uniformly). For a fixed ice load geometry, the Farrell & Clark (1976) theory is linearly related to the

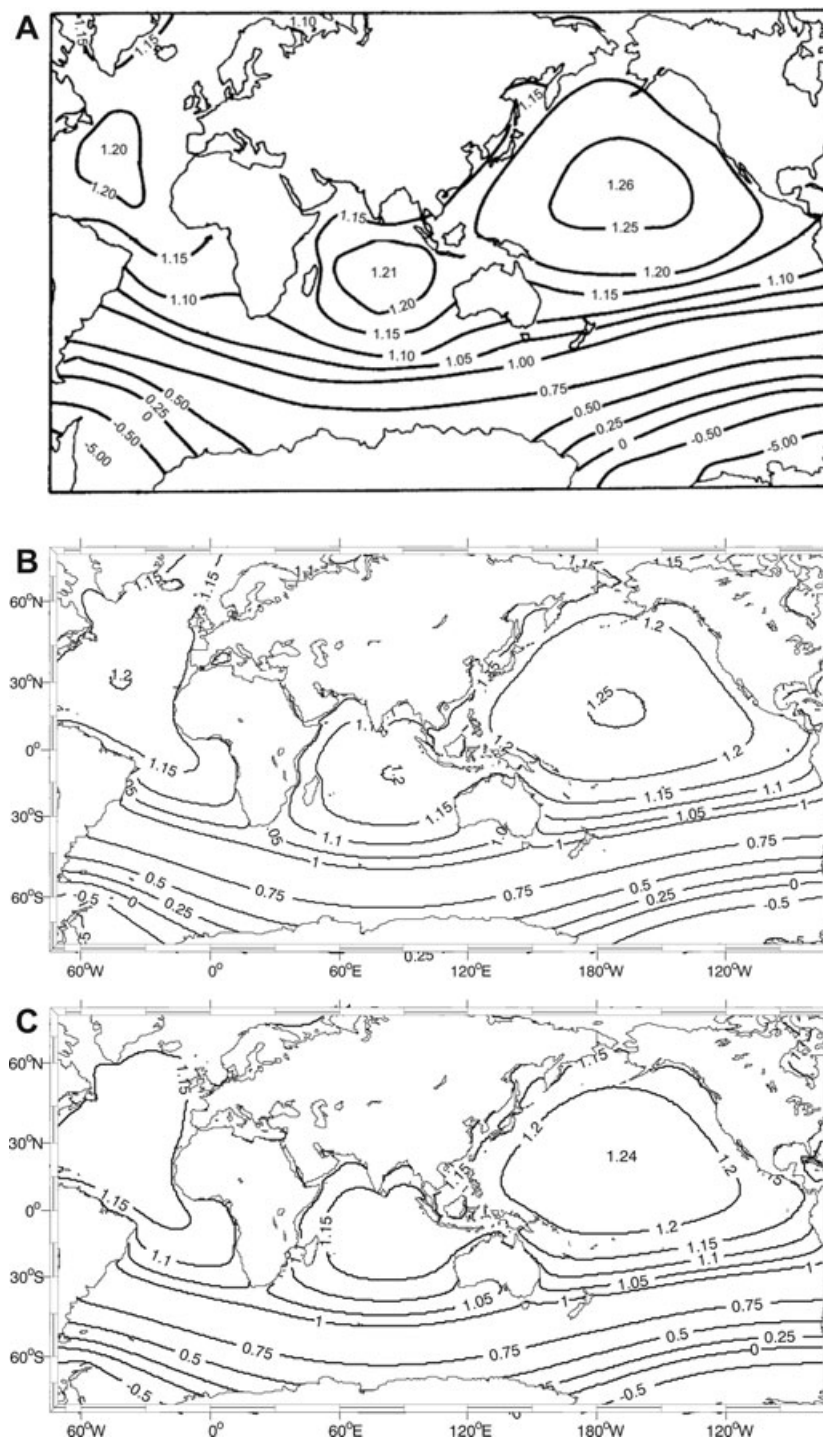


Figure 1. Sea level fingerprints for a rapid, uniform thinning across the WAIS, normalized by the eustatic sea level change. All calculations assume a fixed shoreline, no rotational feedback, and a 1-D elastic earth model. (a) Result reproduced from Clark & Lingle (1977). Their calculation involved a Love-number based, space-domain Green's function sea level solver described by Clark *et al.* (1978) (method GFS in Section 2.4) and it adopted a Gutenberg-Bullen model for the Earth's elastic and density structure. (b) Fingerprint computed using a Love-number based pseudo-spectral solution (Mitrovica & Peltier 1991) (method PSS in Section 2.4) of the sea level eqs (22)–(23) with a truncation at spherical harmonic degree and order 512, and the earth model PREM (Dziewonski & Anderson 1981). (c) Fingerprint computed using the space-domain solver 3DS (Section 2.4) of the generalized sea level eqs (7)–(9) applied to the special (fixed shoreline, no rotational feedback) case treated in Section 2.1 (eqs 13–15). 3DS is based on a finite-volume formulation of the Earth's elastic response (Latychev *et al.* 2005) and in these calculations we adopt the earth model PREM.

total ice flux, and therefore the normalized map of sea level change computed by Clark & Lingle (1977) can be scaled to consider any case of uniform melting (or growth) of the WAIS. The map shows a peak sea level rise greater than 25 per cent above the eustatic value

in the north Pacific and more than 20 per cent above the eustatic in the north Atlantic and Indian Oceans. In addition, the sea level fall is greater than five times the eustatic amplitude in the ocean adjacent to the West Antarctic.

With the exception of a follow-up study by Clark & Primus (1987), the spatially variable pattern of sea level change following the rapid melting of ice reservoirs was largely overlooked in analyses of modern global sea level rise (e.g. Peltier & Tushingham 1989; Douglas 1991, 1997) until a suite of studies revisited the issue beginning in the late 1990s (Conrad & Hager 1997; Mitrovica *et al.* 2001; Plag & Jüttner 2001; Tamisiea *et al.* 2001; Plag 2006). Since mass changes in a specific ice sheet or glacier produce a distinct geometry of sea level change, these geometries have come to be known as sea level ‘fingerprints’.

There is now widespread recognition that geographic variability in sea level trends provides for the possibility of constraining (or fingerprinting) the sources of the meltwater, and this has motivated a significant reappraisal of observed trends. As an example, Mitrovica *et al.* (2001) demonstrated that the geographic variation in sea level rates evident at two dozen tide gauge sites adopted by Douglas (1997) could be reconciled by a specific combination of various fingerprints associated with mass flux from polar ice sheets and mountain glaciers, including an inferred 20th century melt rate in Greenland equivalent to a eustatic sea level rise of $\sim 0.5 \text{ mm yr}^{-1}$. The study was considered to be preliminary in the sense that the geometry of the steric effect of ocean thermal expansion was unknown and treated as uniform. Plag (2006) analysed a global database of tide gauge trends using a fingerprinting approach and inferred an equivalent eustatic sea level contribution of 0.39, 0.10 and 0.35 mm yr^{-1} over the last 50 yr from the Antarctic and Greenland ice sheets and steric effects, respectively.

Mitrovica *et al.* (2001) and Tamisiea *et al.* (2001) used an extended sea level equation that included the impact of a contemporaneous perturbation in the Earth’s rotation vector. In more recent work investigating the sea level fingerprint associated with the possible future collapse of the WAIS (Mitrovica *et al.* 2009; Gomez *et al.* 2010), the theory was further extended to incorporate changes in shoreline geometry associated with local onlap or offlap of water and with changes in the extent of grounded, marine-based ice sheets. In an independent analysis using an approximate treatment of shoreline migration, Bamber *et al.* (2009) also predicted the fingerprint of WAIS collapse.

Despite the increased interest in sea level fingerprints, progress in the field has been hindered by ongoing suggestions of a major flaw in the numerical calculation of the fingerprints. These suggestions are based on the discrepancy between fingerprints predicted by Mitrovica *et al.* (2001) and Plag & Jüttner (2001). Most recently, the issue was highlighted by Vellinga *et al.* (2008), who in a study of the hazard posed by sea level change in the Netherlands, wrote: ‘At present, the causes for the large differences in fingerprints presented by Mitrovica *et al.* (2001) . . . and Plag and Jüttner (2001) . . . are not fully explained. . . The causes of these differences are thought to be either in the way the sea level equation is solved or in different model assumptions, such as incorporation of variations in Earth rotation’ (p. 31). The discrepancy between the studies cited in the quote is large. As an example, melting from the Antarctic was predicted to lead to a sea level rise in the Netherlands of 1.1 times the eustatic value by Mitrovica *et al.* (2001) and 2.6 times the eustatic value by Plag & Jüttner (2001). Moreover, these studies predicted a sea level change in the Netherlands of 0.2 and -2.5 times the eustatic value, respectively, in the case of Greenland melting.

In this paper, we address the issue of the robustness of numerically predicted sea level fingerprints. First, we provide an analytic sea level solution for the case of the melting of ice on a non-rotating elastic Earth with global oceans and compare this solution to the analogous rigid-Earth case. We also compare both solutions

to results generated using the standard pseudo-spectral numerical algorithm (Mitrovica & Peltier 1991; Kendall *et al.* 2005; Gomez *et al.* 2010) adopted within the post-glacial sea level community. Next, we summarize two comparative studies of published sea level predictions. The first comparison involves the fingerprint of moderate thinning of the WAIS computed by Clark & Lingle (1977) using a ‘Green’s Function’ (space-domain) sea level code (Fig. 1a) and fingerprints for this case generated by independent pseudo-spectral and space-domain solvers of the governing sea level equation. In the second comparison, we explore differences in the sea level fingerprint of WAIS collapse published by Mitrovica *et al.* (2009) and Bamber *et al.* (2009).

The paper ends with two sensitivity analyses. The above results, and indeed all previously published studies, assume a 1-D (i.e. depth varying) elastic earth model. We perform the first fingerprint calculations on earth models that include lateral variations in density and elastic structure and assess the sensitivity of the predictions to the inclusion of this level of complexity. Previous fingerprint calculations have also generally assumed a simple, uniform melt geometry from the polar ice sheets. We conclude the study by presenting predictions based on spatially variable melt geometries constrained from analyses of GRACE Tellus products (Chambers 2006). A comparison with uniform-melt fingerprints will establish to what extent future efforts to estimate meltwater contributions from modern sea level records must consider more realistic melt geometries.

This study is intended as guidance to those researchers who are citing sea level fingerprinting results and also those interested in computing such fields. To this end, upon publication of this work we will make available online numerical software capable of generating a fingerprint on a rotating, 1-D elastic earth model given an arbitrary, user-specified melt geometry. As progressively more geodetic data related to ice mass flux and sea level data become available, the need for publically accessible tools for computing fingerprints is overdue.

2 THE SEA LEVEL EQUATION

In this section, we briefly summarize the derivation of the generalized sea level equation appearing in Mitrovica & Milne (2003) and Kendall *et al.* (2005). Our aim is to highlight special cases of the equation adopted in the various studies discussed below, as well as to present some analytic results useful for benchmarking purposes.

We define sea level, SL , as a global field equal to the difference between the radial height of the sea surface and the solid surface, where the latter excludes the height of grounded ice. Also, we define topography as the negative of this field

$$T(\theta, \psi, t) = -SL(\theta, \psi, t), \quad (1)$$

where θ and ψ are the colatitude and east longitude of a site and t is time. The ocean height is simply related to global sea level by

$$S(\theta, \psi, t) = SL(\theta, \psi, t) \cdot C^*(\theta, \psi, t), \quad (2)$$

where the projection operator, the ocean function C^* , is defined as

$$C^*(\theta, \psi, t) = \begin{cases} 1 & \text{if } SL(\theta, \psi, t) > 0 \text{ and there is no grounded ice} \\ 0 & \text{elsewhere.} \end{cases} \quad (3)$$

We will be concerned with changes in sea level from some initial state $t = t_0$. Accordingly, we may write

$$\begin{aligned} SL(\theta, \psi, t) &= SL(\theta, \psi, t_0) + \Delta SL(\theta, \psi, t), \\ T(\theta, \psi, t) &= T(\theta, \psi, t_0) + \Delta T(\theta, \psi, t) \\ &= T(\theta, \psi, t_0) - \Delta SL(\theta, \psi, t), \\ C^*(\theta, \psi, t) &= C^*(\theta, \psi, t_0) + \Delta C^*(\theta, \psi, t). \end{aligned} \quad (4)$$

The perturbation in the ocean height, ΔS , may be computed by taking the difference between the expression (2) at times t and t_0 . After some straightforward algebra, this exercise yields (Mitrovica & Milne 2003)

$$\begin{aligned} \Delta S(\theta, \psi, t) &= \Delta SL(\theta, \psi, t) \cdot C^*(\theta, \psi, t) \\ &\quad - T(\theta, \psi, t_0) \cdot \Delta C^*(\theta, \psi, t). \end{aligned} \quad (5)$$

The distinction between sea level and ocean height is important because, while perturbations to sea level may be defined globally, only changes in ocean height, ΔS , act to load the planet. In this regard, eq. (5) has a simple physical explanation. The first term on the right-hand side is the projection of the change in global sea level onto the ocean function at time t , while the second term is the correction of the ocean height necessary to account for a migration of the shoreline (due to either onlap or offlap or changes in the extent of grounded ice) between t and t_0 .

ΔSL is commonly decomposed into a spatially variable component, which we denote as $\Delta S\mathcal{L}$ and a globally uniform shift. Hence, we can write

$$\Delta SL(\theta, \psi, t) = \Delta S\mathcal{L}(\theta, \psi, t) + \frac{\Delta\Phi(t)}{g}. \quad (6)$$

Postglacial sea level changes are computed using a so-called static (or equilibrium) sea level theory in which the sea surface is constrained to remain on an equipotential (Farrell & Clark 1976). However, it is important to note that the specific equipotential that defines the sea surface may vary over time as mass is added or removed from the ocean and/or the solid surface adjusts to the loading (see Dahlen (1976) for an elegant discussion of this physics in the case of long-period ocean tides). The second term on the right-hand side of eq. (6), which includes the surface gravitational acceleration g , is a function of the change in the defining equipotential from its initial value (we denote this change as $\Delta\Phi$). This term is computed, as we describe below, by invoking conservation of mass of the surface load.

In this paper, we are concerned with the sea level change just after the rapid melting of an ice reservoir, where the term ‘rapid’ is used to denote a change in the ice load that occurs faster than the Maxwell time of the viscoelastic earth model. Thus our calculations are performed for a single time step away from the initial ($t = t_0$) state, and they treat the earth model as elastic. In this regard, the time dependence in the above equations will henceforth be dropped and the symbol Δ will denote a perturbation across the single (before and after loading) time step.

The spatially variable sea level change, $\Delta S\mathcal{L}$, is driven by changes in the surface mass load, which includes variations in ice height (which we will denote by ΔI) and ocean height (ΔS), and by perturbations in the Earth’s rotation vector (henceforth $\Delta\omega$). It will be instructive to rewrite eq. (5) in a form which makes the dependencies of $\Delta S\mathcal{L}$ explicit, while also making the dependencies on the spatial co-ordinates and time implicit

$$\Delta S = \left[\Delta S\mathcal{L}(\Delta I, \Delta S, \Delta\omega) + \frac{\Delta\Phi}{g} \right] \cdot C^* - T_0 \cdot \Delta C^*, \quad (7)$$

where we have used eq. (6). The subscript 0 on the topography term denotes an initial value. Eq. (7) is the generalized sea level equation derived by Mitrovica & Milne (2003). It is clear from this expression that the sea level equation is an integral equation; this integral form reflects the fact that changes in ocean height perturb the gravitational field, but they are in turn governed by the gravitational field since the sea surface must remain an equipotential.

We complete this derivation by integrating both sides of eq. (7) over the surface of the Earth (Ω), multiplying by the density of water (ρ_w), and invoking conservation of mass in the total surface (ice plus water) load. This yields the following expression for $\Delta\Phi/g$

$$\begin{aligned} \frac{\Delta\Phi}{g} &= -\frac{1}{\mathcal{A}} \frac{\rho_i}{\rho_w} \iint_{\Omega} \Delta I \, d\Omega \\ &\quad - \frac{1}{\mathcal{A}} \iint_{\Omega} \Delta S\mathcal{L}(\Delta I, \Delta S, \Delta\omega) \cdot C^* \, d\Omega \\ &\quad + \frac{1}{\mathcal{A}} \iint_{\Omega} T_0 \cdot \Delta C^* \, d\Omega, \end{aligned} \quad (8)$$

where ρ_i is the density of ice and \mathcal{A} , given by

$$\mathcal{A} = \iint_{\Omega} C^* \, d\Omega, \quad (9)$$

is the total area of (grounded) ice-free oceans after the rapid melting event. In deriving this equation, we have made use of the mass conservation equation

$$\rho_w \iint_{\Omega} \Delta S \, d\Omega + \rho_i \iint_{\Omega} \Delta I \, d\Omega = 0. \quad (10)$$

Solving the sea level eqs (7)–(9) requires a numerical methodology for computing perturbations in global sea level arising from changes in the surface mass load and the rotation vector, that is, $\Delta S\mathcal{L}$. For 3-D earth models, this calculation can be performed by using spectral, finite element or finite volume software that have recently been developed to consider GIA on such models (e.g. Martinec 2002; Wu & van der Wal 2003; Zhong *et al.* 2003; Latychev *et al.* 2005). For 1-D earth models, $\Delta S\mathcal{L}$ is typically computed using a spectral analysis (e.g. Kendall *et al.* 2005) ultimately based on viscoelastic Love number theory (Peltier 1974).

Finally, we derive an expression for the eustatic sea level change, defined as the uniform change in global sea level under the assumption of a non-rotating ($\Delta\omega = 0$) and rigid earth model in which self-gravitation of the surface load is neglected ($\Delta S\mathcal{L} = 0$). In this case

$$\begin{aligned} \Delta SL^{\text{eus}} &= \frac{\Delta\Phi^{\text{eus}}}{g} \\ &= -\frac{1}{\mathcal{A}^{\text{eus}}} \frac{\rho_i}{\rho_w} \iint_{\Omega} \Delta I \, d\Omega + \frac{1}{\mathcal{A}^{\text{eus}}} \iint_{\Omega} T_0 \cdot \Delta C^{*,\text{eus}} \, d\Omega, \end{aligned} \quad (11)$$

where the superscript ‘eus’ denotes a change computed under the assumption of eustasy and

$$\mathcal{A}^{\text{eus}} = \iint_{\Omega} C^{*,\text{eus}} \, d\Omega, \quad (12)$$

2.1 Fixed shorelines, no rotational feedback

In this section, we consider the special case of the generalized sea level equation in which shorelines are assumed to be fixed in time. That is, no shoreline migration associated with either changes in the extent of grounded, marine-based ice or onlap or offlap arising from local sea level changes, are considered. In essence we assume

that all shorelines are steep vertical cliffs. We will also neglect the feedback of perturbations in Earth rotation onto sea level.

Setting $C^* = C_0$, $\Delta C^* = 0$ and $\Delta\omega = 0$ in the generalized sea level eq. (7)–(9) yields

$$\Delta S = \left[\Delta \mathcal{S} \mathcal{L}(\Delta I, \Delta S) + \frac{\Delta \Phi}{g} \right] \cdot C_0 \quad (13)$$

and

$$\frac{\Delta \Phi}{g} = -\frac{1}{\mathcal{A}_0} \frac{\rho_i}{\rho_w} \iint_{\Omega} \Delta I \, d\Omega - \frac{1}{\mathcal{A}_0} \iint_{\Omega} \Delta \mathcal{S} \mathcal{L}(\Delta I, \Delta S) \cdot C_0 \, d\Omega, \quad (14)$$

where \mathcal{A}_0 is given by

$$\mathcal{A}_0 = \iint_{\Omega} C_0 \, d\Omega. \quad (15)$$

The eustatic sea level rise in this case is given by

$$\Delta SL^{\text{eus}} = \frac{\Delta \Phi^{\text{eus}}}{g} = -\frac{1}{\mathcal{A}_0} \frac{\rho_i}{\rho_w} \iint_{\Omega} \Delta I \, d\Omega. \quad (16)$$

The system of eqs (7)–(9) or (13)–(15) are valid for earth models of arbitrary complexity. In the case of a 1-D earth models, we can make use of Love number theory to derive a spectral form of the above sea level equation. We treat this issue in the next section.

2.2 Fixed shoreline, no rotational feedback, 1-D elastic Earth

Any scalar field defined over the surface of the Earth can be expressed in terms of a spherical harmonic expansion. As an example, the spatially varying component of the global sea level change may be written as

$$\Delta \mathcal{S} \mathcal{L}(\Delta I, \Delta S) = \sum_{\ell=1}^{\infty} \sum_{m=-\ell}^{\ell} \Delta \mathcal{S} \mathcal{L}_{\ell m}(\Delta I, \Delta S) Y_{\ell m}(\theta, \psi), \quad (17)$$

where the $Y_{\ell m}$ are spherical harmonic basis functions of degree ℓ and order m . We adopt the following normalization for these basis functions

$$\iint_{\Omega} Y_{\ell' m'}(\theta, \psi) Y_{\ell m}^*(\theta, \psi) \sin \theta \, d\theta \, d\psi = 4\pi a^2 \delta_{\ell' \ell} \delta_{m' m}, \quad (18)$$

where the asterisk represents a complex conjugation and a is the mean radius of the Earth.

One can then show, using elastic Love number theory, that the spherical harmonic coefficients of the global sea level change are (Kendall *et al.* 2005)

$$\Delta \mathcal{S} \mathcal{L}_{\ell, m}(\Delta I, \Delta S) = \tau_{\ell} E_{\ell} [\rho_i \Delta I_{\ell m} + \rho_w \Delta S_{\ell m}], \quad (19)$$

where

$$\tau_{\ell} = \frac{4\pi a^3}{M_e(2\ell + 1)} \quad (20)$$

and

$$E_{\ell} = 1 + k_{\ell}^E - h_{\ell}^E. \quad (21)$$

In these equations, $\Delta I_{\ell m}$ and $\Delta S_{\ell m}$ are the spherical harmonic coefficients of the change in the ice height and ocean height, respectively, M_e is the mass of the Earth, and h_{ℓ}^E and k_{ℓ}^E are the elastic h and k Love numbers at spherical harmonic degree ℓ (Farrell 1972). The first two terms on the right-hand side of eq. (21) incorporate the warping of the original sea-surface equipotential due to load self-gravitation

and load-induced deformation, respectively. The third term represents crustal deformation; that is, the load-induced displacement of the bottom bounding surface of sea level.

Using eqs (17) and (19) in the sea level eqs (13)–(15) yields

$$\Delta S = \left(\sum_{\ell=1}^{\infty} \sum_{m=-\ell}^{\ell} \tau_{\ell} E_{\ell} [\rho_i \Delta I_{\ell m} + \rho_w \Delta S_{\ell m}] Y_{\ell m}(\theta, \psi) + \frac{\Delta \Phi}{g} \right) \cdot C_0 \quad (22)$$

and

$$\frac{\Delta \Phi}{g} = -\frac{1}{C_{0(0,0)}} \left(\frac{\rho_i}{\rho_w} \Delta I_{0,0} + \mathcal{R} \mathcal{O}_{0,0} \right), \quad (23)$$

where the field $\mathcal{R} \mathcal{O}$, and the associated spherical harmonics $\mathcal{R} \mathcal{O}_{\ell m}$, are defined as

$$\Delta \mathcal{R} \mathcal{O} = \Delta \mathcal{S} \mathcal{L}(\Delta I, \Delta S) \cdot C_0 = \sum_{\ell=0}^{\infty} \sum_{m=-\ell}^{\ell} \Delta \mathcal{R} \mathcal{O}_{\ell m} Y_{\ell m}(\theta, \psi). \quad (24)$$

Setting $\Delta \mathcal{S} \mathcal{L} = 0$ gives the eustatic sea level change in this case

$$\Delta SL^{\text{eus}} = \frac{\Delta \Phi^{\text{eus}}}{g} = -\frac{1}{C_{0(0,0)}} \frac{\rho_i}{\rho_w} \Delta I_{0,0}. \quad (25)$$

2.3 Fixed shoreline, no rotational feedback, 1-D elastic Earth, global ocean

We can use the results of the last section to consider a further special case in which the ocean covers the entire surface of the planet. This case permits an analytic solution that will be useful as a benchmark result that we (and future sea level modellers) can use to test the accuracy of numerical software.

A global ocean cover means that $C_0(\theta, \psi) = 1$ and thus

$$C_{0\ell, m} = \begin{cases} 1 & \text{if } \ell = 0 \text{ and } m = 0 \\ 0 & \text{for all other harmonics.} \end{cases} \quad (26)$$

Using this in eqs (22)–(25) yields

$$\begin{aligned} \Delta S &= \Delta SL(\Delta I, \Delta S) \\ &= \sum_{\ell=1}^{\infty} \sum_{m=-\ell}^{\ell} \tau_{\ell} E_{\ell} [\rho_i \Delta I_{\ell m} + \rho_w \Delta S_{\ell m}] Y_{\ell m}(\theta, \psi) + \frac{\Delta \Phi}{g} \end{aligned} \quad (27)$$

and

$$\frac{\Delta \Phi}{g} = \Delta SL^{\text{eus}} = \Delta S^{\text{eus}} = -\frac{\rho_i}{\rho_w} \Delta I_{0,0}. \quad (28)$$

Eq. (27) can be solved analytically to give:

$$\Delta S = \Delta SL = \sum_{\ell=1}^{\infty} \sum_{m=-\ell}^{\ell} \left[\frac{\tau_{\ell} E_{\ell} \rho_i}{1 - \tau_{\ell} E_{\ell} \rho_w} \right] \Delta I_{\ell m} Y_{\ell, m}(\theta, \psi) - \frac{\rho_i}{\rho_w} \Delta I_{0,0}. \quad (29)$$

If we normalize this result by the eustatic sea level change given by eq. (28), we obtain:

$$\frac{\Delta S}{\Delta S^{\text{eus}}} = \frac{\Delta SL}{\Delta SL^{\text{eus}}} = 1 - \sum_{\ell=1}^{\infty} \sum_{m=-\ell}^{\ell} \left[\frac{\tau_{\ell} E_{\ell} \rho_w}{1 - \tau_{\ell} E_{\ell} \rho_w} \right] \frac{\Delta I_{\ell m}}{\Delta I_{0,0}} Y_{\ell, m}(\theta, \psi). \quad (30)$$

Thus the second term on the right-hand side of eq. (30) provides the (normalized) departure of sea level from the eustatic approximation.

If an axisymmetric load is placed at the North Pole, the normalized sea level change becomes

$$\frac{\Delta S}{\Delta S^{\text{eus}}} = \frac{\Delta SL}{\Delta SL^{\text{eus}}} = 1 - \sum_{\ell=1}^{\infty} \left[\frac{\tau_{\ell} E_{\ell} \rho_w}{1 - \tau_{\ell} E_{\ell} \rho_w} \right] \frac{\Delta I_{\ell,0}}{\Delta I_{0,0}} Y_{\ell,0}(\theta, \psi), \quad (31)$$

where the $Y_{\ell,0}$ are simply Legendre polynomials of degree ℓ and order zero and thus axisymmetric.

Our results may be seen as an extension of the problem treated by Woodward (1888) to the case of an elastic, rather than rigid Earth, and an arbitrary surface mass load. In this regard, we can consider two further special cases of eq. (30). First, for a rigid Earth, the term E_{ℓ} is replaced by unity and in this case the perturbation in the sea-surface equipotential arises from self-gravitation alone:

$$\left(\frac{\Delta S}{\Delta S^{\text{eus}}} \right)^{\text{rigid}} = \frac{\Delta SL}{\Delta SL^{\text{eus}}} = 1 - \sum_{\ell=1}^{\infty} \left[\frac{\tau_{\ell} \rho_w}{1 - \tau_{\ell} \rho_w} \right] \frac{\Delta I_{\ell,0}}{\Delta I_{0,0}} Y_{\ell,0}(\theta, \psi), \quad (32)$$

Second, for a δ -function load placed at the pole, the term $\Delta I_{\ell,0}/\Delta I_{0,0}$ is replaced by $Y_{\ell,m=0}(\theta=0, \psi=0)$ in eq. (31) or (32).

The derivations in Sections 2.2 and 2.3 are analogous to classic treatments of the Earth's equilibrium ocean tides, as reviewed, for example, by Dahlen (1976).

2.4 Numerical algorithms

Several distinct algorithms have been developed to solve various forms of the sea level equation. We will review their basic elements here.

Farrell & Clark (1976) (see also Clark & Lingle 1977; Clark *et al.* 1978) solved the sea level equation for fixed shorelines, no rotational feedback, and a 1-D Earth. Specifically, they used an approach in which perturbations in global sea level, $\Delta S\mathcal{L}$, were computed by expressing the required spatial convolution of the (ice plus water) load with the sea level Green's function as a sum of signals from discs of various sizes and distances from the observation point. This disc-discretization of the load imposed, for example, higher resolution of the water load at shorelines than in the open ocean. (For viscoelastic calculations a convolution and discretization of the temporal response was also required.) This space-domain approach for computing $\Delta S\mathcal{L}$ was used within an iterative algorithm in which the integral sea level eqs (13)–(15) in Section 2.1 was solved by successively improving a first guess to the ocean redistribution, ΔS . We will henceforth call this approach the Green's function sea level solver (GFS).

Mitrovica & Peltier (1991) also assumed fixed-shorelines, no rotational feedback and a 1-D earth model. To avoid space-domain discretizations, they developed the spectral approach in Section 2.2, whereby the surface load was expressed in terms of spherical harmonics and the spatial convolution between this load and the sea level Green's function was performed analytically. Two independent equations were developed to solve the resulting system of equations. The first was a purely spectral solution that required a matrix inversion and involved no iterative component. We will call this the fully spectral solver (FSS). The second was an iterative pseudo-spectral solver (PSS) in which all calculations were performed spectrally, with the exception of the projection of global sea level, ΔSL , onto the ocean function (eq. 22), which was carried out in the space-domain. The iteration, as in the GFS algorithm, was used to successively refine a first guess to the ocean load ΔS in the solution of the integral eq. (22). [The first guess to ΔS is plugged

into the right-hand side of eq. (22) and the equation is solved for ΔS , which serves as the next guess, and the procedure is repeated until a convergence criterion for ΔS is satisfied.] Both the FSS and the PSS, as well as the GFS, were developed to solve the general viscoelastic problem, but their simplification to consider the purely elastic case poses no difficulty.

The PSS has become the standard sea level solver in the case of 1-D elastic and viscoelastic earth models. In this regard, the algorithm has been extended on two occasions since its original development. The first extension incorporated rotational effects in the spectral expressions for the global sea level change, $\Delta S\mathcal{L}$ (Milne & Mitrovica 1998). A second extension was required to treat time-varying shorelines (Johnston 1993; Milne *et al.* 1999; Kendall *et al.* 2005). We will label the Kendall *et al.* (2005) treatment of the latter as the extended pseudo-spectral solver (EPSS).

All four methods described above (GFS, FSS, PSS and EPSS) are limited to the case of sea level changes on 1-D earth models, since they ultimately all adopt Love number theory to treat the Earth response to surface loads. The recent development of numerical methods capable of treating more complex, 3-D earth models (e.g. Wu & van der Wal 2003; Zhong *et al.* 2003; Latychev *et al.* 2005) requires general sea level solvers. Kendall *et al.* (2005) has described an iterative, space-domain numerical scheme suitable for predicting sea level changes on 3-D models, based on the solution of eqs (7)–(9). We will call this algorithm 3DS.

The only algorithm that will not be directly tested in the results below will be the FSS approach. However, the original derivation of this algorithm by Mitrovica & Peltier (1991) demonstrated that the approach yielded the same results as the PSS algorithm when a consistent spherical harmonic truncation was adopted.

3 RESULTS

All calculations described herein, with the exception of those reproduced from published results by other groups, will be based on earth models which adopt the elastic and density structure of the seismically inferred model PREM (Dziewonski & Anderson 1981). This choice is the case for both the 1-D and 3-D earth model solutions; in the case of the latter, the PREM profiles provide the depth-averaged variation of the fully 3-D structure. In the case of the former, the PREM structure is embedded within the elastic Love number combination E_{ℓ} (eq. 21) that appears in the various versions of the sea level equation appropriate for 1-D earth models (e.g. 22, 27 and 30). To assist future benchmarking exercises we show, in Fig. 2, E_{ℓ} for spherical harmonic degrees up to 512.

3.1 Benchmarking with analytic expressions

To begin, we consider the sea level eqs (27)–(28), which are valid for global oceans and no rotational feedback on a 1-D elastic (or, with E_{ℓ} set to 1, rigid) Earth. Since an analytic solution exists for this special case (eq. 30), this example provides a useful check on the accuracy and convergence of pseudo-spectral numerical solvers.

We will consider an ice load modelled as a single, axisymmetric disc of radius 10° centred at the North Pole. The disc has a parabolic vertical cross-section, and the height of the disc is chosen such that the total mass is equivalent to a eustatic sea level rise of 1 m. The analytic solutions for this axisymmetric case, given by eq. (31) for a 1-D elastic Earth, and eq. (32) for a rigid Earth, are shown by the solid black lines labelled 'Elastic' and 'Rigid', respectively, in Fig. 3. The analogous coloured lines are results generated using the

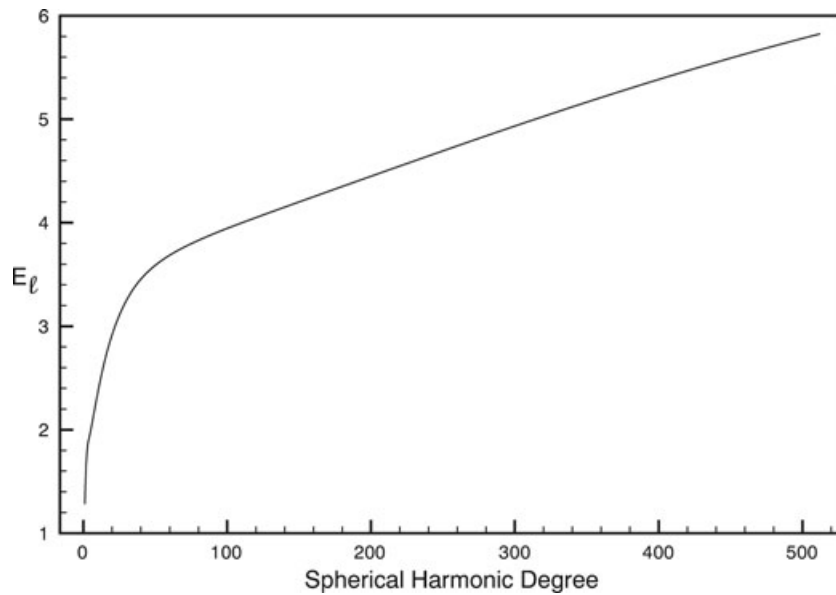


Figure 2. The elastic Love number combination E_ℓ (eq. 21) as a function of spherical harmonic degree ℓ computed using the 1-D elastic and density structure given by the seismic model PREM (Dziewonski & Anderson 1981).

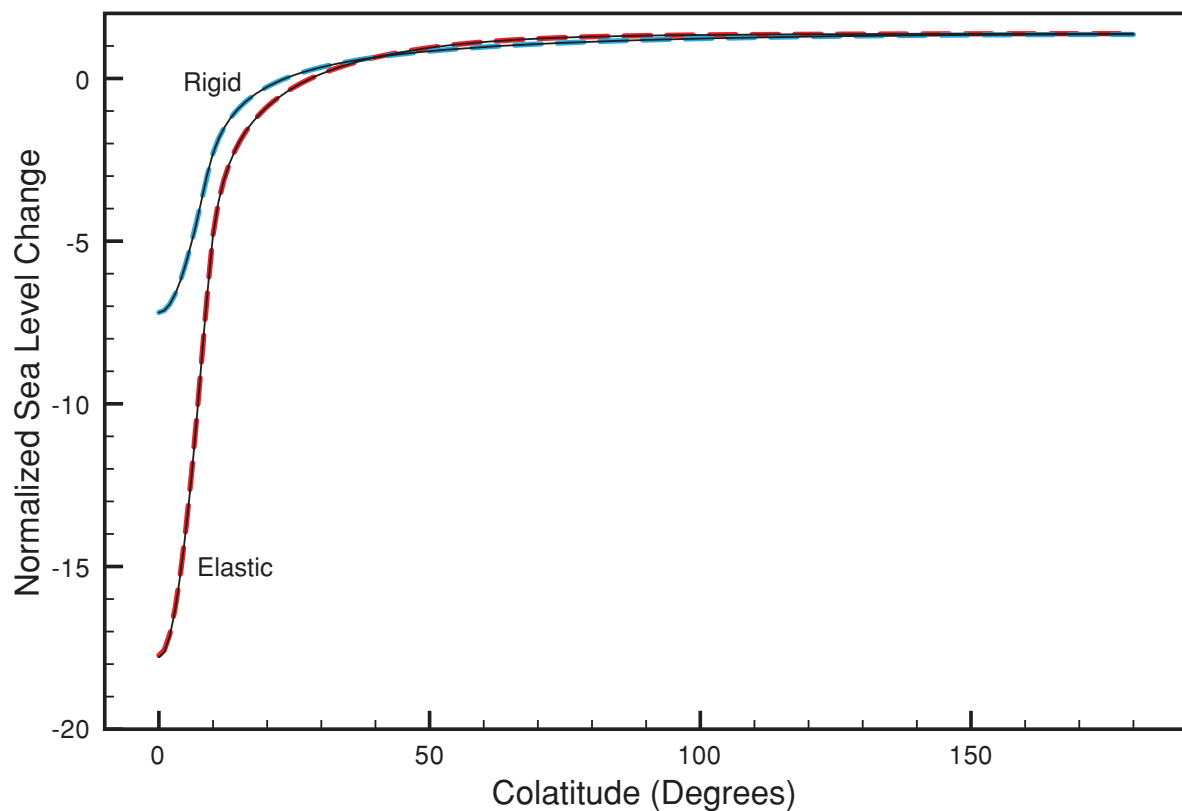


Figure 3. A comparison of sea level fingerprints computed under the assumption of a global ocean and no rotational feedback and normalized using the eustatic sea level change. The calculations adopt a parabolic disc load of radius 10° with center at the North Pole, and the axisymmetric fingerprint is thus plotted as a function of colatitude only. The dashed blue line and the underlying solid black line correspond to predictions based on a rigid Earth model; the dashed red line and underlying black line are analogous results for an elastic Earth model (the elastic Love number combination E_ℓ for the latter pair is shown in Fig. 2). In each case, the coloured lines are solutions based on a pseudo-spectral solution (Mitrovica & Peltier 1991) of the sea level eqs (27)–(28) (method PSS in Section 2.4). The black lines are the fingerprints computed from the associated analytic solutions valid for a rigid (eq. 32) or 1-D elastic (eq. 31) earth model. All solutions adopt a truncation at degree and order 512.

pseudo-spectral sea level solver applied to the sea level eqs (27)–(28). The PSS is initiated by adopting a first guess to the sea level change, which is taken to be the equivalent eustatic value of the melt, and it iteratively improves upon this guess until convergence (Mitrovica & Peltier 1991; Kendall *et al.* 2005). The PSS predictions in Fig. 3 have clearly converged to the correct solution and the robustness of the methodology is thus demonstrated.

The rigid earth model calculations in Fig. 3 are consistent with the results of Woodward (1888), who treated the case of a δ -function loading. In particular, the profiles show a sea level fall within ~ 2000 km of the melting ice disc and a far field sea level rise that exceeds the eustatic value by ~ 35 per cent. The elastic results show comparable values in both these respects. However, the elastic fingerprint exhibits a somewhat broader (by 500 km) region of sea level fall, which reflects the added contribution to this signal from elastic uplift within a large zone surrounding the disc load. Moreover, this same deformation contribution yields a peak sea level fall which is approximately two to three times larger than the rigid case in the near field of the ice sheet. Nevertheless, despite these differences, it is significant to note that the far field sea level rise is very similar in both the elastic and rigid Earth cases.

3.2 Clark & Lingle (1977)

Clark & Lingle (1977) predicted the normalized sea level fingerprint associated with a uniform thinning of the WAIS on a 1-D elastic and non-rotating earth model with realistic ocean geometry (Fig. 1a). Their calculation was based on the iterative Green's function sea level solver, GFS, described above, and their elastic Love numbers were computed using what they described as a Gutenberg–Bullen earth model. The Green's functions they adopted were computed up to very high degree and order ($\ell \gg 1000$), and so the resolution of their prediction was governed by the spatial discretization of the ice geometry and ocean load, which was highly variable.

The existence of this classic prediction serves as a useful target for comparison. To this end, in Fig. 1(b) we show our prediction of the normalized sea level fingerprint generated using the PSS algorithm applied to the sea level eqs (22)–(23). We adopted a truncation at degree and order 512 and the elastic Love number combination E_ℓ shown in Fig. 2. To facilitate comparison, the new figure is drawn using the same projection and contour levels as the original. The agreement between the two techniques is excellent, with peak positive values in the north Pacific, Indian and Atlantic Oceans matching the Clark & Lingle (1977) prediction to within 1 per cent. We emphasize that this consistency is achieved despite differences in: (1) the numerical methodology used to solve the sea level eq. (GFS versus PSS); (2) the 1-D elastic earth model (Gutenberg–Bullen versus PREM) and (3) the numerical software used to compute the elastic Love numbers.

Because both calculations are based on a Love number formalism, it would be useful to provide an additional calculation that does not share this characteristic. To this end, in Fig. 1(c) we show a prediction of the normalized sea level fingerprint generated from a calculation in which: (1) Earth's 1-D elastic response to the surface mass load (i.e. $\Delta S\mathcal{L}$) is computed using a finite-volume numerical formulation of the governing field equations described in detail in Latychev *et al.* (2005); and (2) the sea level equation is solved using an iterative, space-domain sea level solver (3DS in Section 2.4). The finite-volume computational (tetrahedral) grid used in the Earth response calculation involves a total of ~ 15 million nodes with variable spatial resolution. In particular, the grid has 56 spherical

layers extending from the core-mantle-boundary to the surface, and a radial and lateral resolution that ranges from 25 to 50 km in the upper mantle to 70–20 km in the lower mantle. The surface is discretized with a resolution of about 15 km. All aspects of the calculation in Fig. 1(c) are independent of the numerical approaches used to generate the other frames in the figure, and the agreement is, once again, excellent.

The results in Figs 1 and 3 show consistency across calculations that include three different algorithms for the solving the sea level equation, PSS, GFS and 3DS, as well as an analytic solution, in addition to two fundamentally different techniques for computing the Earth's elastic response to a surface mass load—Love number theory and a finite-volume numerical scheme. The predictions in Fig. 1 concur that the normalized sea level fingerprint of WAIS thinning on a non-rotating, 1-D elastic Earth with fixed shorelines, has a far field sea level rise that peaks ~ 20 – 25 per cent above the eustatic value. Moreover, the results in Fig. 3 indicate that this level of amplification will not be strongly impacted even by the assumption of a rigid earth model. We conclude, on this basis, that the results presented by Plag & Jüttner (2001), which predict an amplification of 2.6 times the eustatic value in the Netherlands, in the case of melting from the Antarctic ice sheet (in contrast to a factor of 1.1 predicted in all three frames of Fig. 1), are erroneous.

3.3 Sea level projections

In the last year, two independent studies have predicted the normalized sea level change associated with the potential future collapse of the WAIS (Bamber *et al.* 2009; Mitrovica *et al.* 2009). The sea level fingerprints in these two publications were roughly consistent, though discrepancies in the peak magnitudes have raised questions concerning the robustness of such predictions. In this section, we revisit these analyses in an attempt to reconcile these discrepancies.

Mitrovica *et al.* (2009) presented a sea level fingerprint of WAIS collapse (reproduced in Fig. 4a) computed by solving the generalized sea level eqs (7)–(9) using the EPSS algorithm (Section 2.4) and normalizing the result by the 'effective eustatic value' (EEV) of the melting. The EEV was determined by converting grounded portions of the WAIS into water, infilling all marine-based sectors of the region with water, and redistributing the remaining meltwater uniformly across the oceans. (The latter redistribution defined the EEV). The fingerprint was computed (and normalized) using a scenario of total WAIS collapse (EEV = 5 m). The peak sea level rise in Fig. 4(a), which occurs in the northeast Pacific off the west coast of North America, represents a 37 per cent amplification above the EEV. In contrast, while the Bamber *et al.* (2009) fingerprint was characterized by a peak in the same area, their amplitude was only ~ 25 per cent above the EEV.

The Bamber *et al.* (2009) fingerprint was computed under the assumption that only a portion of the WAIS, equivalent to an EEV of 3.3 m, would collapse in any future warming scenario. The question arises as to whether this difference in the melting scenario (all of the WAIS versus partial collapse) is responsible for the discrepancy in the peak amplitude. This would be surprising since the quasi-linear relationship between the surface load and the sea level response means that the same fingerprint should be reasonably accurate for any scenario in which significant marine-based ice cover collapses. To confirm this assumption, Fig. 4(b) shows the result of a new calculation, identical in all regards to the Mitrovica *et al.* (2009) prediction except that only grounded ice within marine-based sectors of the WAIS (EEV ~ 3.5 m) is assumed to melt. The difference

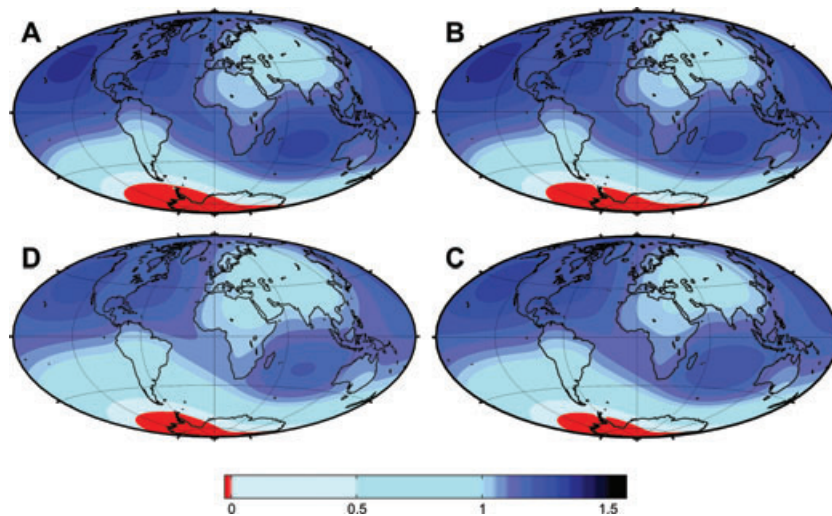


Figure 4. (a) Normalized (by the EEV) sea level fingerprint of WAIS collapse published by Mitrovia *et al.* (2009). The prediction is based on the EPSS algorithm applied to the generalized sea level eqs (7)–(9), and it assumes that all grounded sectors of the WAIS collapse ($EEV = 5$ m). (b) As in (a), except the fingerprint (and normalization) is computed from a sea level calculation in which only grounded marine-based sectors of the WAIS collapse ($EEV = 3.5$ m). (c) As in (b), except that the solid Earth deformation is computed using an elastically incompressible rheology. (d) As in (c), except that water expulsion within the WAIS is turned off.

in the peak sea level amplification evident in Figs 4(a) and (b) (order 0.001) is clearly negligible and we must look to other causes for the discrepancy between the Mitrovia *et al.* (2009) and Bamber *et al.* (2009) results.

As described above, underlying all calculations of sea level change in response to the rapid collapse of an ice sheet is a model for the elastic deformation of the solid Earth associated with the surface mass and rotational potential forcing. The solid Earth is elastically compressible. However, in computing this component of the sea level response, Bamber *et al.* (2009) adopted a simplified earth model that was elastically incompressible. The model adopted in Mitrovia *et al.* (2009), and in all the calculations in Figs 1–3, was compressible. In Fig. 4(c) we repeat the calculation in Fig. 4(b), with the exception that we switch off compressibility in the elastic response. Adopting an incompressible model significantly reduces the deformational response of the solid Earth relative to the compressible case. As an illustrative example, the radial uplift in Ellsworth Land in the West Antarctic predicted using the incompressible model is 60 per cent lower than the prediction based on a compressible model (4.5 m versus 12.1 m). The net impact of this dampened crustal deformation is a significantly lower predicted sea level fall in the near field of the ice sheet (e.g. a ~ 40 per cent underprediction at Ellsworth Land) and a predicted peak sea level amplification in the northeast Pacific that drops to 32 per cent of the EEV. Thus, the simplified rheology adopted by Bamber *et al.* (2009) accounts for about half of the discrepancy between the two groups cited above.

Because Mitrovia *et al.* (2009) applied the EPSS algorithm to the generalized sea level eqs (7)–(9) (Kendall *et al.* 2005), their calculation takes into account both rotational feedback and the migration of shorelines. Both processes are important in the case of the WAIS; the latter is significant because a collapse of the WAIS would lead to an expulsion of water from marine-based sectors of the region as they uplift in response to the ice unloading (Mitrovia *et al.* 2009; Gomez *et al.* 2010). The Bamber *et al.* (2009) study adopted a PSS sea level algorithm that incorporated all these effects except water expulsion. In particular, in calculating their normalized sea level fingerprint they assumed that no marine-based sectors of the West

Antarctic are exposed and no water expulsion occurs—this is their ‘partial collapse’ scenario. We have repeated the (incompressible) calculation in Fig. 4(c) with the exception that we added the further assumption that none of the WAIS is marine-based (Fig. 4d). The normalized fingerprint we obtain is now a very close match to the Bamber *et al.* (2009) projection (see their fig. 4)—in particular, the peak amplification is close to 27 per cent in both cases.

To treat the case of ‘full collapse’ Bamber *et al.* (2009) performed an ‘*a posteriori*’ procedure in which they computed the mean sea level fall over regions that are uplifting due to the ice unloading and which are known to be presently marine-based in the West Antarctic. Next, they took the meltwater volume associated with this integrated sea level fall and spread it uniformly over the oceans. Finally, they augmented the EEV of the WAIS collapse by this uniform rise, and this augmented EEV was used to dimensionalize their normalized (i.e. partial collapse) fingerprint. As the numerical example for Ellsworth Land cited above illustrates, the factor they computed as an add-on to the EEV (6 cm) was an underestimate because of the assumption of incompressibility. In any case, the Bamber *et al.* (2009) method of incorporating a ‘full collapse’ into the predictions is not gravitationally self-consistent since it assumes that the water expulsion leads to a uniform (eustatic) rise in sea level. This assumption leads to a prediction of sea level rise in regions like the U.S. coastlines that is less than the correct treatment of water expulsion would yield (Mitrovia *et al.* 2009; Gomez *et al.* 2010).

We conclude that projections of future sea level rise should be computed using a complete sea level theory. In the context of the goals of this paper, we also conclude that even relatively small discrepancies in fingerprints published by most groups can be understood and explained through a careful analysis of the physics underlying the predictions.

3.4 Sensitivity analyses

3.4.1 Sea level fingerprints on 3-D elastic earth models

To date, all predictions of sea level fingerprints have been based on 1-D elastic earth models. To consider the sensitivity of these

predictions to lateral variations in elastic structure in this section we compare the results of 1-D and 3-D elastic earth models for the case of a non-rotating Earth with fixed shorelines.

We will consider loading scenarios in which a uniform layer of mass is removed from either the Greenland or the West Antarctic Ice Sheets. To be consistent, all calculations (1-D and 3-D) are performed using the 3DS algorithm (as in Fig. 1c) to solve for the sea level eqs (13)–(14). The models assume a depth averaged elastic and density structure given by PREM. The 3-D Earth model has lateral shear and compressional wave speed variations that are given by seismic models S16B30 and P16B30, respectively (Bolton 1996; Masters *et al.* 1996); to prescribe lateral variations in density, we assume that the ratio of relative perturbations in density and shear wave speed is 0.4 (Bolton 1996).

In Fig. 5 we show predictions of normalized sea level fingerprints computed for the 1-D and 3-D earth models, as well as their difference (i.e. 3-D – 1-D), for both melting scenarios. In contrast, for example, to the sensitivity of the predictions to the adoption of compressible versus incompressible elastic rheology (Fig. 4), the introduction of 3-D elastic structure has a negligible impact on the predictions. (We have confirmed this insensitivity using a suite of other 3-D earth models based on seismic models S20RTS (Ritsema *et al.* 2004) and SPRD6 (Ishii & Tromp 2001).) The largest perturbations are seen in the near field, within the melt zone: In the West Antarctic case, the (normalized) differences range from -0.04 to 0.07 over the ice sheet, and in the Greenland case this range is -0.10 to 0.01 . These are less than ~ 1 per cent of the total normal-

ized near field sea level fall (~ 20 times the eustatic value), which is roughly the same order as the perturbations in elastic structure from PREM associated with the 3-D model. We conclude that future analyses of modern sea level data sets need not take into account this level of earth model complexity.

3.4.2 Geometry of melt

Previous predictions of the sea level fingerprints of melting from polar ice sheets – including most of those described above—have generally adopted simplified models of the geometry of ice mass flux; for example, melting that is uniform, proportional to ice height or spatially limited to the ice sheet perimeter (for an exception, see Wake *et al.* 2006). However, recent analyses of GRACE satellite-gravity data have provided detailed estimates of regional variations in the polar mass flux (e.g. Velicogna & Wahr 2005; Chen *et al.* 2006; Velicogna & Wahr 2006; Chen *et al.* 2007). In this section, we predict normalized fingerprints based on GRACE-inferred melt geometries over both the Antarctic and Greenland, and compare these to analogous fingerprints computed under the assumption of uniform mass loss over Greenland and the West Antarctic. All calculations are performed using the pseudo-spectral algorithm for solving the generalized sea level eqs (7)–(9) valid for a rotating earth model with time varying shorelines (EPSS; Kendall *et al.* 2005). The goal is not to provide updated fingerprints, since GRACE analyses suggest that the detailed geometry of polar ice mass flux is

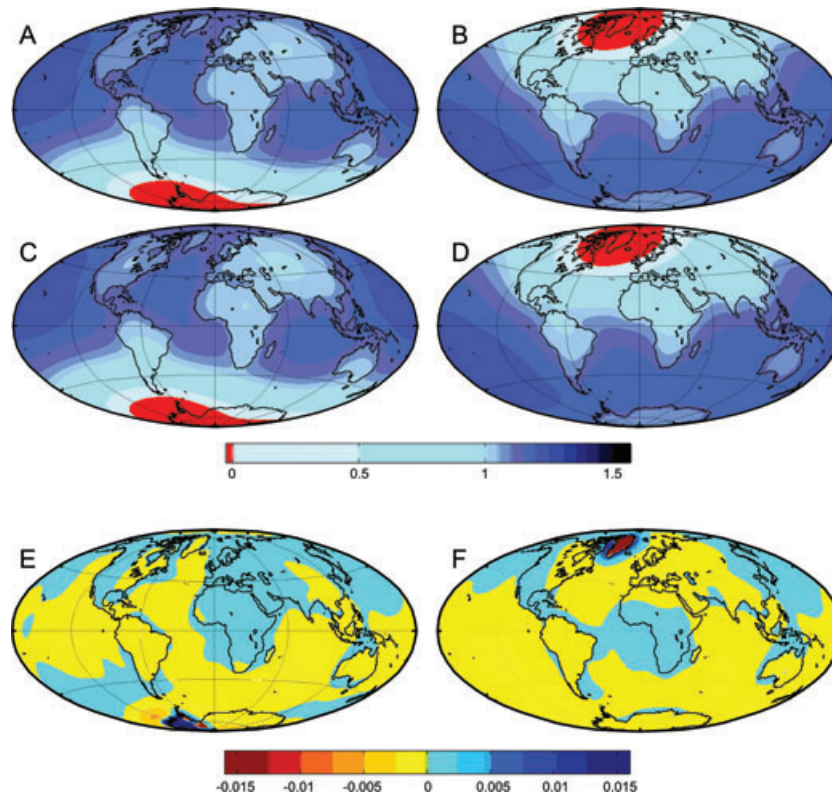


Figure 5. Sea level fingerprints for uniform thinning of the (a) WAIS and (b) Greenland Ice Sheet, computed under the assumption of fixed shorelines, no rotational feedback and 1-D elastic and density structure prescribed from the model PREM (Dziewonski & Anderson 1981). Frame A is identical to Fig. 1(c). (c) and (d) are analogous to (a) and (b), respectively, with the exception that a 3-D elastic earth model is adopted (see text). Panel (e) and (f) show differences between the 1-D and 3-D predictions, i.e. 3-D minus 1-D result, for WAIS and Greenland thinning, respectively. All fingerprints are computed using a space-domain solver of the sea level eq. (13)–(15) (method 3DS in Section 2.4) and are based on a finite-volume formulation of the Earth's elastic response (Latychev *et al.* 2005).

continually evolving; rather, it is to establish the broad sensitivities to be expected in the evolving patterns of sea level change.

We will denote the uniform West Antarctic and Greenland melt scenarios by WA-U and G-U, respectively. The next load model is based on the Antarctic mass flux geometry inferred, through forward modelling, by Chen *et al.* (2007, see their Fig. 3) using GRACE data collected from 2003 January to 2006 September. The geometry (Fig. 6a; henceforth WA-V) is comprised of six distinct, localized zones of mass flux: (1) the northern Antarctic Peninsula; (2) south-

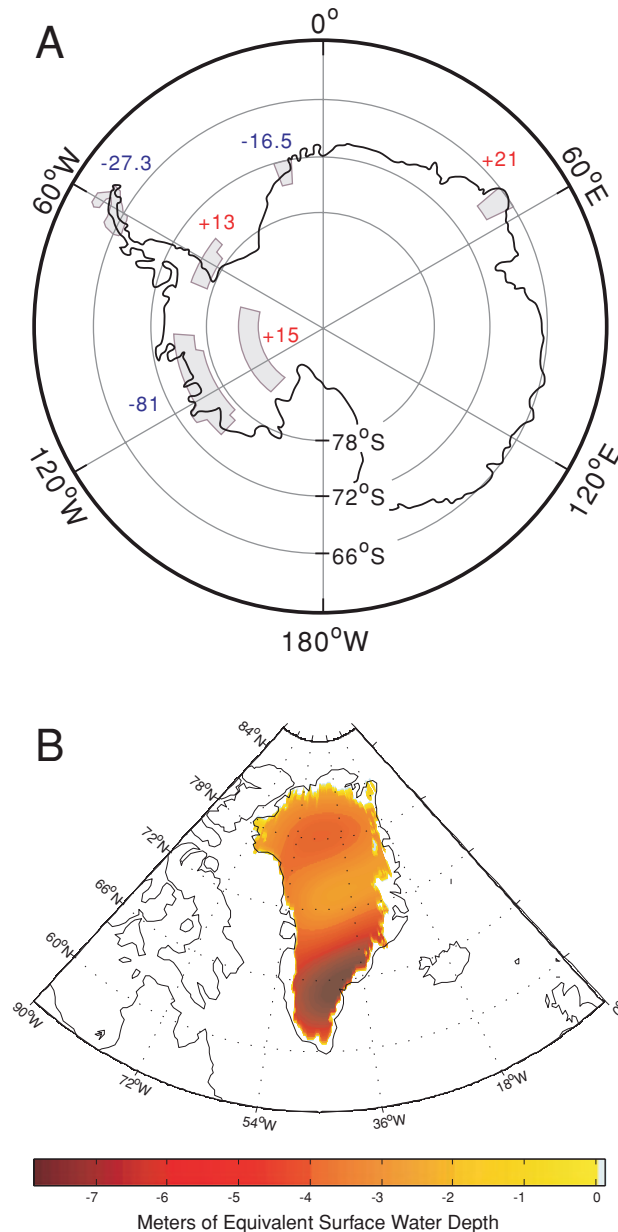


Figure 6. (a) Melt model inferred by Chen *et al.* (2007) from GRACE satellite gravity measurements. The figure shows six zones of mass flux (1-6; see text), and the mass rates are given in units of $\text{km}^3 \text{yr}^{-1}$. The total mass rate is equivalent to a eustatic sea level rise of 0.23 mm yr^{-1} . (b) The mass balance trend (in meters of equivalent surface water depth per year) estimated using GRACE data from 2002–2009 over the Greenland Ice Sheet (see text). The melt model is derived by zeroing out all regions outside Greenland and scaling the resulting geometry to yield 1 mm yr^{-1} of eustatic sea level rise.

eastern Antarctic Peninsula; (3) the Amundsen Sea; (4) the central West Antarctic, north of the Whitmore Mountains; (5) Dronning Maud Land and (6) Scott Mountains. The net mass loss from the first four of these regions, all within the WAIS and the Antarctic Peninsula, is a factor of ~ 18 greater than the net GRACE-inferred mass gain from the two East Antarctic sites. This dominance of WAIS flux justifies our decision to compare results generated using the model WA-V with the uniform melt scenario WA-U. The total mass loss is equivalent to a eustatic sea level rise of 0.23 mm yr^{-1} .

The next melt model we consider, G-V, was generated from our own analysis of the GRACE data set. Specifically, a linear trend was calculated from an unweighted least-squares fit to monthly mass grids provided by GRACE Tellus data spanning 2003 January to 2009 January (Chambers 2006). The GRACE Tellus data were pre-processed with the degree 2, order 0 coefficients replaced by satellite laser ranging estimates and a postglacial rebound signal removed (by A. Paulson) using the ICE-5G deglaciation history with the VM2 earth model (Peltier 2004). The mass grids were destriped and smoothed with a 300 km half width filter. The melt model (Fig. 6b) was generated by zeroing all anomalies outside Greenland and scaling the remaining field to yield an equivalent eustatic sea level rise of 1 mm yr^{-1} .

Fig. 7 shows the normalized fingerprints computed for load models G-U, G-V and their difference. The patterns in Figs 7(a) and (b) are qualitatively similar, though Fig. 7(c) reveals two underlying contributions to the difference. First, in the near field, the difference plot indicates a dipole pattern with an axis through central Greenland. This dipole arises from a southward shift of the melt geometry, and hence the near field zone of sea level fall, in the G-V model relative to the G-U case (Fig. 6b). The pattern has an (normalized) amplitude that far exceeds the scale of the colour bar: -5.1 to 2.3 . Indeed, the amplitude of the difference exceeds the eustatic value well outside of the melt zone. In the far field there is a small amplitude pattern that is also related to the southward shift of the melt geometry. Specifically, the model G-U yields a displacement of the rotation pole towards Greenland (37°W) of 116 mm per mm of equivalent eustatic sea level (ESL) rise. Melt model G-V excites a slightly larger polar motion (125 mm per mm of ESL), in the same direction, which is as one would expect given that the mass flux in this model is offset further from the rotation pole than in model G-U. As a result, the quadrantal geometry of sea level change associated with rotational feedback (Milne & Mitrovica 1998), which in the case of Greenland melting leads to a sea level rise in Asia and southern South America and a sea level fall over Australia and the north Atlantic, is amplified. This amplification is very small, amounting to less than 2 per cent of the eustatic value.

The sensitivity to melt geometry is even stronger in the Antarctic case (Fig. 8). In this melt scenario, the fingerprints in Figs 8(a) and (b) show qualitative differences within both the near and far field, and this is reflected in Fig. 8(c). First, since the melt model (A-V) brings the main deglaciation centres closer to the margin of the WAIS, the polar motion (in the direction 98°W) excited by the melt is twice as large as in model A-U (188 mm versus 97 mm , per mm of ESL). This larger displacement yields an increase in the amplitude of the rotational feedback signature equal to ~ 10 per cent of the eustatic value. The geometry of this feedback signature is such that it produces a sea level rise over North America and the southern Indian Ocean and a fall over Asia and southern South America.

In the near field, the difference in the fingerprints exhibits a strong dipole structure that adds to the rotational feedback signal in the southern hemisphere; at the centre of the deep blue and red regions (off the west coast of Chile, and between Africa and Australia,

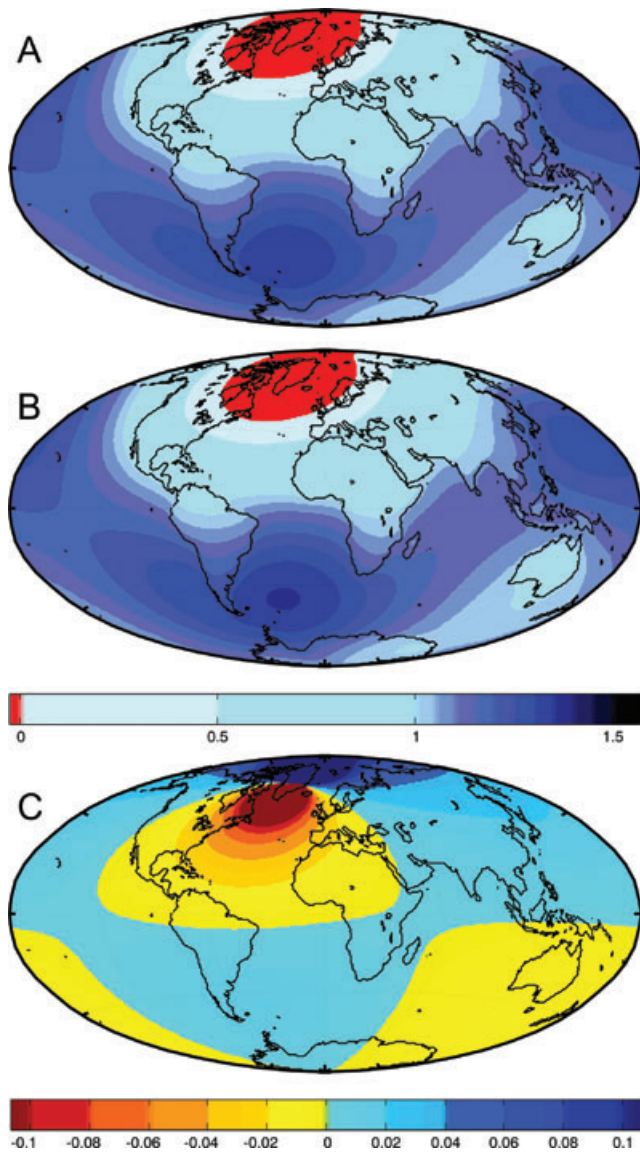


Figure 7. Normalized sea level fingerprints computed using melt models (a) G-U, (b) G-V and (c) their difference (i.e. frame b minus a). The melt model G-V is shown in Fig. 6(b).

respectively) the amplitude of the difference is ~ 0.4 , or 40 per cent of the eustatic value. Closer to, but outside Antarctica, the difference exceeds the eustatic value, and within the melt zone the difference can be over an order of magnitude greater than the eustatic value.

4 FINAL REMARKS

We have presented a comparative analysis of the sea level fingerprints of rapid ice sheet melting computed using a number of numerical methods and based on earth models and sea level theories of varying complexity.

As an example, a comparison of a pseudo-spectral calculation of the sea level change in a global (i.e. no continent) ocean due to rapid melting of the WAIS with an analytic solution demonstrated that pseudo-spectral sea level solvers, which are the most common algorithms for computing deglaciation-induced sea level change, converge to the correct solution (Fig. 3). Furthermore, we were able to reproduce to within ~ 1 per cent accuracy peak values of the

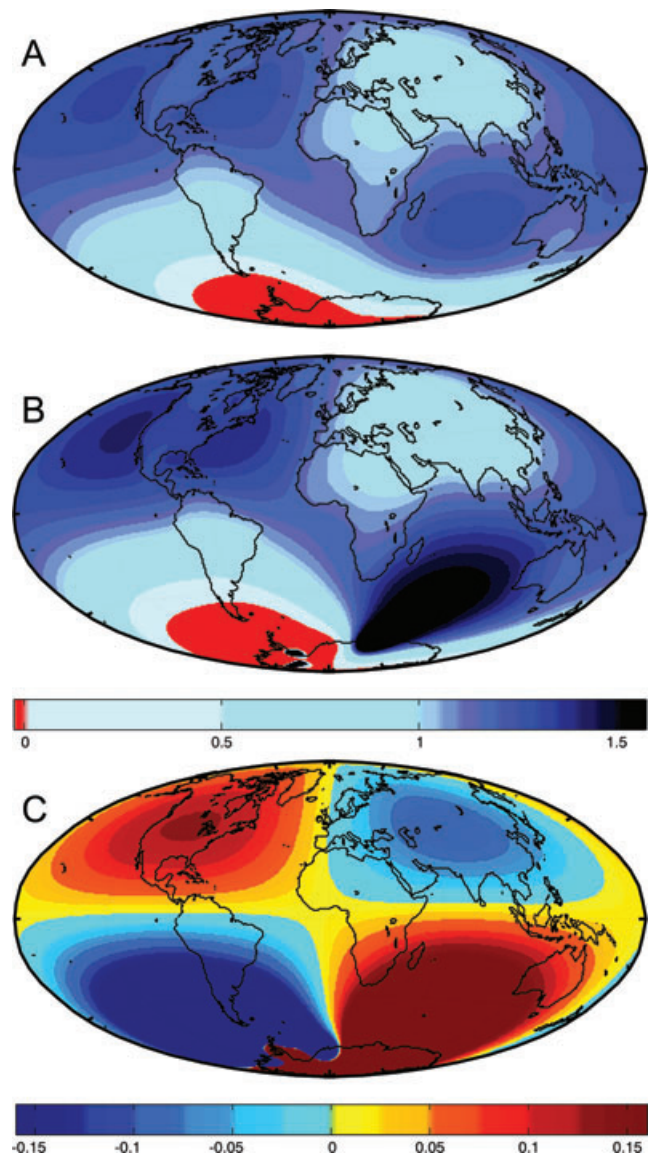


Figure 8. Normalized sea level fingerprints computed using melt models (a) WA-U, (b) WA-V and (c) their difference (i.e. frame b minus a). The melt model WA-V is shown in Fig. 6(a).

sea level fingerprint associated with uniform melting of the WAIS published by Clark & Lingle (1977) for the case of a non-rotating, 1-D elastic earth model with fixed, present-day ocean geometry and a Green's function sea level solver (Fig. 1). The agreement was evident in comparisons with solutions computed using a pseudo-spectral solver based on both a 1-D Love number formulation and a space-domain solver based on a 3-D finite volume code for predicting the Earth's elastic response to loading.

One of the most pressing applications of fingerprint studies is the projection of future sea level changes following the collapse of existing reservoirs of ice. We have presented a detailed comparison of two recent projections involving the potential collapse of the WAIS (Bamber *et al.* 2009; Mitrovica *et al.* 2009; Gomez *et al.* 2010) which were based on rotating earth models with evolving shoreline geometry. The projections by Mitrovica *et al.* (2009) and Gomez *et al.* (2010) are characterized by a peak far field sea level amplification relative to the eustatic trend of ~ 37 per cent, which is significantly higher than the 25 per cent amplification factor

predicted by Bamber *et al.* (2009). We have demonstrated that this difference is due to two approximations adopted by Bamber *et al.* (2009); namely, their use of an incompressible elastic rheology and a eustatic treatment of water expulsion from uplifting, marine-based sectors of the WAIS subsequent to ice sheet collapse.

The consistency associated with predictions using three different sea level solvers, two independent approaches to computing the Earth's response to loading (Love number and finite volume), two 1-D elastic earth models (PREM and Guttenberg-Bullen), and numerical versus analytic approaches, as well as our ability to understand the causes of the discrepancy between recent sea level projections, demonstrates the robustness of most predictions of sea level fingerprints. This consistency also highlights the discordant nature of fingerprint calculations presented by Plag & Jüttner (2001) and Plag (2006), which, for example, predict a normalized far field sea level rise that is a factor of two larger than the value predicted by any other method or study cited above (2.6 versus ~ 1.3). We conclude that the discordance is due to an unknown error in the Plag & Jüttner (2001) and Plag (2006) analyses.

In the second part of the paper, we presented an investigation of the sensitivity of sea level fingerprints to the inclusion of 3-D elastic Earth structure and spatially variable melt geometries inferred from the analysis of GRACE gravity observations. Not surprisingly, the GRACE-based fingerprints differed significantly from analogous uniform-melt fingerprints in the near field of the polar ice sheets. Perhaps more surprisingly, these differences remained significant into the far field in the case of Antarctic melting. The far field sensitivity in this case originates from the rotational feedback signal. Specifically, since the Antarctic ice sheet covers the South Pole, relatively modest changes in melt geometry can produce significant changes in the amplitude and orientation of the polar motion driven by the mass flux. We conclude that analyses of modern sea level changes should, where possible, incorporate constraints on the geometry of polar ice mass changes. In contrast, our predictions based on 3-D elastic earth models indicate that lateral variations in elastic Earth structure need not be included in future studies.

Numerical (Fortran) software based on the PSS algorithm, and capable of computing a sea level fingerprint on a rotating, 1-D (PREM-based) elastic earth model given an arbitrary, user-specified melt geometry, is available online at: http://www.psmsl.org/train_and_info/geo_signals/fingerprints/pseudo_spectral_1D/

ACKNOWLEDGMENTS

GRACE data were processed by D. P. Chambers, supported by the NASA Earth Science REASON GRACE Project, and are available at <http://grace.jpl.nasa.gov>. We thank two anonymous reviewers for constructive comments. JXM acknowledges support from Harvard University and the Canadian Institute for Advanced Research.

REFERENCES

Bamber, J.L., Riva, R.E.M., Vermeersen, L.L.A. & LeBrocq, A.M., 2009. Reassessment of the potential sea-level rise from a collapse of the West Antarctic Ice Sheet, *Science*, **324**, 901–903.

Bolton, H., 1996. Long Period Travel Times and the Structure of the Mantle, *PhD thesis*, Univ. California, San Diego.

Chambers, D.P., 2006. Evaluation of new GRACE time-variable gravity data over the ocean, *Geophys. Res. Lett.*, **33**, L17603, doi:10.1029/2006GL027296.

Chen, J.L., Wilson, C.R. & Tapley, B.D., 2006. Satellite gravity measurements confirm accelerated melting of Greenland ice sheet, *Science*, **313**, 1958–1960.

Chen, J.L., Wilson, C.R., Tapley, B.D., Blankenship, D. & Young, D., 2008. Antarctic regional ice loss rates from GRACE, *Earth planet. Sci. Lett.*, **266**, 140–148.

Clark, J.A., Farrell, W.E. & Peltier, W.R., 1978. Global changes in postglacial sea level: a numerical calculation, *Quat. Res.*, **9**, 265–287.

Clark, J.A. & Lingle, C.S., 1977. Future sea-level changes due to West Antarctic ice sheet fluctuations, *Nature*, **269**, 206–209.

Clark, J.A. & Primus, J.A., 1987. Sea-level changes resulting from future retreat of ice sheets: an effect of CO₂ warming of the climate, in *Sea-Level Changes*, pp. 356–370, eds Tooley, M.J. & Shennan, I., Institute of British Geographers, London.

Conrad, C. & Hager, B.H., 1997. Spatial variations in the rate of sea level rise caused by present-day melting of glaciers and ice sheets, *Geophys. Res. Lett.*, **24**, 1503–1506.

Dahlen, F.A., 1976. The passive influence of the oceans upon the rotation of the Earth, *Geophys. J. R. astr. Soc.*, **46**, 363–406.

Douglas, B.C., 1991. Global sea level rise, *J. geophys. Res.*, **96**, 6981–6992.

Douglas, B.C., 1997. Global sea rise: A determination, *Surv. Geophys.*, **18**, 279–292.

Dziewonski, A.M. & Anderson, D.L., 1981. Preliminary reference Earth model (PREM), *Phys. Earth planet. Inter.*, **25**, 297–356.

Farrell, W.E., 1972. Deformation of the Earth by surface loads, *Rev. geophys. Space Phys.*, **10**, 761–797.

Farrell, W.E. & Clark, J.A., 1976. On postglacial sea level, *Geophys. J. R. astr. Soc.*, **46**, 647–667.

Gomez, N., Mitrovica, J.X., Tamisiea, M.E. & Clark, P.U., 2010. A new projection of sea level change in response to collapse of marine sectors of the Antarctic Ice Sheet, *Geophys. J. Int.*, **180**, 623–634.

Ishii, M. & Tromp, J., 2001. Even-degree lateral variations in the mantle constrained by free oscillations and the free-air gravity anomaly, *Geophys. J. Int.*, **145**, 77–96.

Johnston, P., 1993. The effect of spatially non-uniform water loads on predictions of sea level change, *Geophys. J. Int.*, **114**, 615–634.

Kendall, R.A., Mitrovica, J.X. & Milne, G.A., 2005. On post-glacial sea level – II. Numerical formulation and comparative results on spherically symmetric models, *Geophys. J. Int.*, **161**, 679–706.

Latychev, K., Mitrovica, J.X., Tromp, J., Tamisiea, M.E., Komatitsch, D. & Christara, C.C., 2005. Glacial isostatic adjustment on 3-D Earth models: a finite volume formulation, *Geophys. J. Int.*, **161**, 421–444.

Martinez, Z., 2000. Spectral-finite element approach to three-dimensional viscoelastic relaxation in a spherical Earth, *Geophys. J. Int.*, **142**, 117–141.

Masters, G., Johnson, S., Laske, G. & Bolton, H., 1996. A shear-velocity model of the mantle, *Phil. Trans. R. Soc. Lond. A*, **354**, 1385–1411.

Milne, G.A. & Mitrovica, J.X., 1998. Postglacial sea-level change on a rotating Earth, *Geophys. J. Int.*, **133**, 1–10.

Milne, G.A., Mitrovica, J.X. & Davis, J.L., 1999. Near-field hydro-isostasy: the implementation of a revised sea-level equation, *Geophys. J. Int.*, **139**, 464–482.

Mitrovica, J.X., Gomez, N. & Clark, P.U., 2009. The sea-level fingerprint of West Antarctic collapse, *Science*, **323**, 753.

Mitrovica, J.X. & Milne, G.A., 2003. On post-glacial sea level: I. General theory, *Geophys. J. Int.*, **154**, 253–267.

Mitrovica, J.X. & Peltier, W.R., 1991. On postglacial geoid subsidence over the equatorial oceans, *J. geophys. Res.*, **96**, 20 053–20 071.

Mitrovica, J.X., Tamisiea, M.E., Davis, J.L. & Milne, G.A., 2001. Polar ice mass variations and the geometry of global sea level change, *Nature*, **409**, 1026–1029.

Peltier, W.R., 1974. The impulse response of a Maxwell Earth, *Rev. Geophys.*, **12**, 649–669.

Peltier, W.R., 2004. Global glacial isostasy and the surface of the ice-age Earth: The ICE-5G (VM2) model and GRACE, *Annu. Rev. Earth planet. Sci.*, **32**, 111–149.

Peltier, W.R. & Tushingham, A.M., 1989. Global sea level rise and the greenhouse effect: might they be connected?, *Science*, **244**, 806–810.

Plag, H.-P. & Jüttner, H.U., 2001. Inversion of global tide gauge data for present-day ice load changes, *Mem. Nat. Inst. Polar Res.*, **54**, 301–318.

Plag, H.-P., 2006. Recent relative sea-level trends: an attempt to quantify the forcing factors, *Phil. Trans. R. Soc.*, **364**, 821–844.

- Ritsema, J., van Heijst, H.J. & Woodhouse, J.H., 2004. Global transition zone tomography, *J. geophys. Res.*, **109**, 10.1029/2003JB002610.
- Tamisiea, M.E., Mitrovica, J.X., Milne, G.A. & Davis, J.L., 2001. Global geoid and sea level changes due to present-day ice mass fluctuations, *J. geophys. Res.*, **106**, 30 849–30 863.
- Velicogna, I. & Wahr, J., 2006. Measurements of time-variable gravity show mass loss in Antarctic, *Science*, **311**, 1754–1756.
- Velicogna, I. & Wahr, J., 2005. Greenland mass balance from GRACE, *Geophys. Res. Lett.*, **32**, L18505, doi:10.1029/2005GL023955.
- Vellinga, P. et al., 2008. Exploring high-end climate change scenarios for flood protection of the Netherlands, *International Scientific Assessment*, Delta Committee, 163pp.
- Wake, L., Milne, G. & Leuliette, E., 2006. 20th century sea-level change along the eastern US: Unravelling the contributions from steric changes, Greenland ice sheet mass balance and Late Pleistocene glacial loading, *Earth planet. Sci. Lett.*, **250**, 572–580.
- Wu, P. & van der Wal, W., 2003. Postglacial sea levels on a spherical, self-gravitating viscoelastic Earth: effects of lateral viscosity variations in the upper mantle on the inference of viscosity contrasts in the lower mantle, *Earth planet. Sci. Lett.*, **211**, 57–68.
- Woodward, R.S., 1888. On the form and position of mean sea level, *US Geol. Surv. Bull.*, **48**, 87–170.
- Zhong, S., Paulson, A. & Wahr, J., 2003. Three-dimensional finite element modeling of Earth's viscoelastic deformation: effects of lateral variations in lithospheric thickness, *Geophys. J. Int.*, **155**, 679–695.